European Journal of Pharmaceutical Sciences 176 (2022) 106247

Contents lists available at ScienceDirect

European Journal of Pharmaceutical Sciences

journal homepage: www.elsevier.com/locate/ejps

Development of extra-fine particles containing nanosized meloxicam for deep pulmonary delivery: *In vitro* aerodynamic and cell line measurements

Petra Party [a], Dávid Kókai [b], Katalin Burián [b], Attila Nagy [c], Béla Hopp [d], Rita Ambrus [a,*]

[a] Institute of Pharmaceutical Technology and Regulatory Affairs, University of Szeged, Eötvös street 6., Szeged 6720, Hungary
[b] Department of Medical Microbiology, Faculty of Medicine, University of Szeged, Dóm square 10., Szeged 6720, Hungary
[c] Wigner Research Centre for Physics, Hungarian Academy of Sciences, Konkoly-Thege Miklós street 29-33., Budapest 1121, Hungary
[d] Department of Optics and Quantum Electronics, University of Szeged, Dóm square 9., Szeged 6720 Hungary

ARTICLE INFO

Keywords:
Dry powder inhaler
Meloxicam
Nano spray-drying
Andersen cascade impactor
Aerodynamic particle counter
A549 cell line

ABSTRACT

Pulmonary drug administration provides a platform for the effective local treatment of various respiratory diseases. Application of nano-sized active ingredients results in higher bioavailability because of their large specific surface area. Extra-fine dry powder inhalers reach the smaller airways, further improving therapeutic efficiency. Poorly water-soluble meloxicam was the selected active ingredient. We aimed to decrease the particle size into the nano range by wet milling and producing extra-fine inhalable particles via nano spray-drying. The diameter of the drug was reduced to 138 nm. The particle size of the dry products was between 1.1 and 1.5 μm, and the dispersed diameter was between 500 and 800 nm. Owing to the excipients (poly-vinyl-alcohol, leucine), the spray-dried particles presented nearly spherical morphology. The drug became partially amorphous. Thanks to the improved surface area, the solubility and the released and the diffused amount of the meloxicam increased in artificial lung media. The *in vitro* aerodynamic measurements showed that the leucine-containing formulations had outstanding fine particle fraction (FPF) deposition with 1.3 μm mass median aerodynamic diameter (MMAD). The aerodynamic particle counter test also proved the extra-fine aerodynamic particle size. The *in vitro* cell line experiments revealed the non-cytotoxicity of the products and the suppression of the interleukin concentration. Overall, the powders are suitable for deep pulmonary delivery and the local treatment of lung inflammations.

1. Introduction

Nanotechnology is currently revolutionizing drug delivery, including the field of pulmonary administration. Its application allows combining the advantages of nanomaterials and the lung as a target. The definition of nanomaterials according to the European Union requires particles size under 100 nm (Potočnik, 2011). Pharmaceutical nanoparticles are defined as individual particles with a size below 1 μm. Typically a mean particle diameter between 200 and 500 nm is applied (Keck and Müller, 2006), (Scherließ et al., 2022). The reduced size and hence larger specific surface area enhance the dissolution rate of poorly water-soluble drugs. Therefore, nanoparticles increase intracellular drug delivery and are better internalized by cells, resulting in higher bioavailability (Muralidharan et al., 2015). Proper formulation is indispensable for the efficient transport of the nanosized active ingredient to the respiratory system. In pulmonary therapy, the generally requested particle size range is aerodynamic particle diameter between 1 and 5 μm. To reach the deeper lung parts, particles 0.5–1.5 μm in size are ideal, because of their very low deposition on their way to the targeted region and their large deposition in the small peripheral lung structures (Heyder, 2004; Thorley and Tetley, 2013; Das et al., 2021). Application of extra-fine particles (< 2 μm) built up nanosized active ingredient could be beneficial for the treatment of deeper lung segments (Hillyer et al., 2018; De Boer et al., 2015; Jetzer et al., 2018; Tse et al., 2021a; Scherließ et al., 2022). Harmonizing the advantages of nanoparticles with the aerodynamics of small microparticles could achieve an improved bioavailability and aerosolization behavior (Malamatari et al., 2020). The extra-fine particles deposit in the alveolar region, where the particles can disperse to nanoparticles. The liberated nano-sized active ingredient can effectively reach the epithelium, because they are not eliminated by the alveolar macrophages's size-dependent uptake (Thorley and Tetley, 2013; Ruge et al., 2013). However, drug delivery efficiency in the

* Corresponding author.
E-mail address: ambrus.rita@szte.hu (R. Ambrus).

https://doi.org/10.1016/j.ejps.2022.106247
Received 11 March 2022; Received in revised form 3 May 2022; Accepted 23 June 2022
Available online 25 June 2022

airways depends not only on the size of the formulations but also on particle morphology, density, and electrical charge (Muralidharan et al., 2015).

The deep respiratory deposition of drugs is important in the treatment of different lung inflammations. For example, in case of the new coronavirus (SARS-CoV-2) infection. When the aerosol particles contact the airways, the virus particles travel down into the acinar airways, resulting in a higher deposition fraction in the acinar airways than in the bronchi (Madas et al., 2020). The virus replicates in type II pneumocytes. After the release of the new virus, it activates alveolar macrophages. The virus also induces the release of proinflammatory cytokines, which leads to the common COVID-19 symptoms: acute respiratory distress syndrome, pneumonia, fever, multiple organ system failure, and coughing (Chugh et al., 2021). Since the virus replicates in alveolar epithelial cells, it is believed that inhaling as deeply as possible will enhance the therapeutic effect of the inhaled drug (Iwabuchi et al., 2020). The direct pulmonary delivery of medicines provides higher lung concentrations as well as reduces systemic toxicity in COVID-19 patients. Dry powder inhalers (DPIs) would be convenient in the therapy. DPIs offer several advantages including ease of use, non-invasiveness, no liquid propellant, an extended-release profile, improved tolerability, and long-term stability (Muralidharan et al., 2015). This approach would be ideal for the treatment of COVID-19 patients in an out-patient setting, especially if COVID-19 becomes a recurrent seasonal disease (Sun, 2020). For the treatment of lung inflammation, cyclooxygenase-2 COX-2) inhibitors could be applied. SARS-CoV-2 infection induces COX-2 expression, which leads to inflammation. Meloxicam (MX) was chosen as an active ingredient during our work, because it is a selective COX-2 inhibitor non-steroidal anti-inflammatory drug (NSAID). The inhibition of COX-2 by MX does not affect viral entry or replication but may play a role in regulating the lung inflammation and injury observed in COVID-19 patients (Chen et al., 2020) . Therefore, MX could be important in the adjuvant therapy of COVID-19 (Ong et al., 2020). Currently, the main indications of MX are arthritis and osteoarthritis in human therapy. MX is commercially available only in oral, intravenous, and intralesional delivery routes (Meloxicam Drugbank). The development of new delivery systems and/or changes in administration routes is an alternative way to reposition drugs. Drug repositioning is widely used by the pharmaceutical industry due to the notable cost and time reduction. An interesting alternative for COVID-19 treatment could be the identification of a suitable repositioned drug to be administered via pulmonary route. The local administration has shown positive results in the treatment of different lung diseases, which may be related to its rapid onset, low metabolic activity, and reduction of adverse effects (Sarcinelli et al., 2021). As previously mentioned, direct lung delivery could be the barely most efficient way to apply the poorly-water soluble MX. Our research group had a widespread experience in the DPI formulation of the drug. Carrier-based DPI-s (Pomázi et al., 2013; Pallagi et al., 2016; Benke et al., 2020) and also carrier-free systems with different structures, such as porous formulations (Chvatal et al., 2019) and "nano-in-micro" particles (Party et al., 2021) were developed containing meloxicam and meloxicam-potassium. Porous formulation also can be delivered into the deeper lung region. They have low density, therefore they make small aerodynamic particle diameter during inhalation (Tse et al., 2021b; Alhajj et al., 2021). "Nano-in-micro" formulations combine the benefits of nanoparticles and microparticles, which leads to achieving better absorption and proper deposition in the lungs (Malamatari et al., 2020; Scherließ et al., 2022).

In the following work, we aimed to further develop our previous research work (Party et al., 2021). Now, we turned the focus to enhancing the water-solubility of the drug and targeting the smaller airways with the extra-fine particles. We selected wet milling to reduce the particle size of the poorly water-soluble MX, which increases the surface area, thus the solubility of the drug improves (Bartos et al., 2018). For the preparation of the inhalable extra-fine powders, we used a nano spray-drying technique. The preparation method is capable of producing particles under 2 μm with narrow distribution and high yields (Li et al., 2010; Arpagaus et al., 2017). In addition, the combination of milling and spray-drying methods is scalable, cost-effective, and environmentally friendly. Besides the physico-chemical characterization and *in vitro* dosage form investigations, we extended the *in vitro* aerodynamic assessment to implement a more accurate characterization of the powders. We also wanted to prove the safety and efficiency of the formulations using *in vitro* cell line tests. Our final goal is to deliver a high percentage of the extra-fine particles into the deeper, alveolar region of the lung, where the nano-sized active ingredient could exert its anti-inflammatory effect. Therefore, we could provide new therapeutic applicability of the MX in the treatment of severe lung inflammation.

2. Materials and methods

2.1. Materials

The active pharmaceutical ingredient (API) was meloxicam (MX) (*Egis Pharmaceuticals PLC., Budapest, Hungary)*. Poly-vinyl-alcohol 4–98 (PVA), *(Aldrich Chemistry, Darmstadt, Germany)* and L-leucine (LEU), *(AppliChem GmbH, Darmstadt, Germany)* were chosen as excipients.

2.2. Methods

2.2.1. Media milling

Firstly PVA was solved in purified water, which resulted in a solution with a 2.5% (w/w%) concentration. PVA is a polymer, which prevents the aggregation of the drug particles during the size reduction. It was followed by the preparation of a presuspension, which contained 2.00 g of pure MX and 18.0 g of 2.5% PVA solution, as a dispersant. A combined wet milling method was used, which was previously optimized by our research group (Bartos et al., 2018; Bartos et al., 2016). The milling medium was 20.00 g of ZrO_2 beads in a planetary ball mill (Retsch Planetary Ball Mill PM 100 MA, Retsch GmbH, Haan, Germany). The milling parameters were the following: 500 rpm, 60 min. After milling, the suspension was diluted to 500 ml with purified water (Party et al., 2021)

2.2.2. Nano spray-drying

Three different compositions were formulated from the MX nanosuspension by adding various amounts of LEU. The dry material contents of the final formulations are shown in Table 1. LEU is an amino acid, which enhances the dispersity of the spray-dried powders. A magnetic stirrer was used for its homogenization in the suspension (*AREC. X heating magnetic stirrer, Velp Scientifica Srl, Italy*). The inhalable powders were produced with a Büchi Nano Spray Dryer equipped with a small nebulizer (*Büchi Nano Spray Dryer B-90 HP, Büchi, Flawil, Switzerland*). Based on our preliminary experiments, the nano spray-drying settings were the following: inlet temperature: 80 °C, aspirator capacity: 100%, airflow rate: 120 ml/min, pump rate: 20%. In all cases, the yield of the nano spray-drying was around 62%. These results exceeded the yield of the traditional spray-drying method (Party et al., 2021).

Table 1
Final composition of the spray-dried samples and the yield of nano spray-drying and composition of the physical mixtures Data are means ± SD (n = 4 independent measurements).

Sample name	MX (g)	PVA (g)	LEU (g)	Yield (%)
nano[MX1_PVA_LEU0]	2.00	0.45	0.00	61.44 ± 3.34
nano[MX1_PVA_LEU0.5]	2.00	0.45	1.00	63.29 ± 2.38
nano[MX1_PVA_LEU1]	2.00	0.45	2.00	62.44 ± 5.86
pm[MX1_PVA_LEU0]	2.00	0.45	0.00	–
pm[MX1_PVA_LEU0.5]	2.00	0.45	1.00	–
pm[MX1_PVA_LEU1]	2.00	0.45	2.00	–

2.2.3. Preparation of the physical mixtures

Three physical mixtures were prepared from the initial materials. Their compositions were equivalent to the nano spray-dried samples (Table 1). During the investigations, the properties of the physical mixtures were compared to the spray-dried products.

2.2.4. Laser diffraction

Laser diffraction was used to determine the particle size, the particle size distribution, and the specific surface area of our samples (Malvern Mastersizer Scirocco 2000, Malvern Instruments Ltd., Worcestershire, United Kingdom). In both cases, the refractive index of MX was adjusted to 1.720. The wet dispersion unit was used to investigate the particle size of the suspension. The suspension was measured in purified water with stirring at 2000 rpm. The dry dispersion unit was used to observe the nano spray-dried powders. The dispersion air pressure was set to 3.0 bar and 75% vibration feed was applied. Each sample was measured in triplicate. The particle size distribution (PSD) was characterized by the values of D[0.1] (10% of the volume distribution is below this value), D [0.5] (50% of the volume distribution is below this value), and D[0.9] (90% of the volume distribution is below this value). Span values were revealed in the particle size distribution, the higher the Span value, the broader the distribution (Li et al., 2004). The specific surface area (SSA) was derived from the PSD data. The calculations were made under the assumption of spherical particles. SSA data predicted the dissolution and diffusion properties of the products.

2.2.5. Dynamic light scattering

The average hydrodynamic diameter (Z-average), polydispersity index (PdI), and zeta potential were analyzed via dynamic light scattering (DLS) using a Malvern Zetasizer Nano ZS (Malvern Instruments, Worcestershire, United Kingdom). The suspension was diluted, the spray-dried formulations were suspended in purified water and measured at 25 °C in folded capillary cells. The refractive index of MX was set to 1.720. Each measurement was carried out in triplicate.

2.2.6. Surface tension measurement

Surface tension measurements of the PVA solution and the MX nanosuspension were carried out using the pendant drop technique with an OCA 20 apparatus (Dataphysics Instrument GmbH, Filderstadt, Germany). The density values of the samples were measured and set for the surface tension calculations. Drop images were collected at 25 °C and the drop profiles were fitted using the Young-Laplace equation (van Eerdenbrugh et al., 2008). For each experiment, ten subsequent images were collected and the average surface tension was used. The experiment was performed in triplicate.

2.2.7. Scanning electron microscopy

Scanning electron microscopy (SEM), (Hitachi S4700, Hitachi Scientific Ltd., Tokyo, Japan) was used to define the morphology of the spray-dried formulations. The investigation conditions were the following: 10 kV high voltage, 10 mA amperage, and 1.3–13.1 mPa air pressure. A high vacuum evaporator and argon atmosphere were applied to make the sputter-coated samples conductive with gold-palladium (Bio-Rad SC 502, VG Microtech, Uckfield, United Kingdom). For the implementation of the particle diameter investigation, ImageJ a public domain image analyzer software was used (https://imagej.nih.gov/ij/index.html).

2.2.8. X-ray powder diffraction

For structural investigation, X-ray powder diffraction (XRPD) spectra were recorded with the help of the BRUKER D8 Advance X-ray diffractometer (Bruker AXS GmbH, Karlsruhe, Germany). The radiation source was Cu Kλ1 radiation (λ=1.5406 Å). The parameters of the analysis were the following: Cu target, Ni filter, 40 kV voltage, 40 mA current, time constant 0.1°/min, angular step 0.010° over the interval of 3–40° DIFFRACT plus EVA 28 software (Bruker AXS GmbH, Karlsruhe, Germany) was used for the evaluation. The crystallinity was calculated via the mean of the decrease of the total area beneath the curve of the characteristic peaks compared with the physical mixtures.

2.2.9. Differential scanning calorimetry

Thermoanalytical properties were determined by differential scanning calorimetry (DSC). The measurements were executed with a Mettler Toledo DSC 821e thermal analysis system with the STARe thermal analysis program V9.1 (Mettler Inc., Schwerzenbach, Switzerland). Approximately 2–5 mg of the samples were observed in the temperature range between 25 °C and 300 °C. The heating rate was 10 °C/min. The carrier gas was argon at a flow rate of 10 l/h during the investigations.

2.2.10. Solubility test

The solubility test of the spray-dried formulations was implemented in simulated lung fluid. It contains 0.68 g/l NaCl, 2.27 g/l NaHCO3, 0.02 g/l CaCl2, 0.1391 g/l NaH2PO4, 0.37 g/l glycine, and 5.56 ml/l 0.1 M H2SO4) (Parlati, 2008). The pH of the medium was 7.4 ± 0.1. A known excess quantity, 15 mg of MX containing powders was added to the media. The samples were stirred with a magnetic stirrer (AREC. X heating magnetic stirrer, Velp Scientifica Srl, Italy) at 25 °C for 24 h and then filtered (pore size=0.45 μm, Millex-HV syringe-driven filter unit, Millipore Corporation, Bedford, USA) and the dissolved drug content was analyzed spectrophotometrically (ATI-Unicam UV/VIS Spectrophotometer, Cambridge, United Kingdom) at a wavelength of 362 nm. The samples were measured in triplicate. Limit of detection (LOD) and limit of quantification (LOQ) was determined for the method as defined in International Conference on Harmonization (ICH) guidelines (ICH Harmonised Tripartite Guideline, 2005), (Prasad and Thireesha, 2018) (The formulas were the following LOD = SD*3.3/S and LOQ = SD*10/S. SD is the standard deviation and S is the mean slope of the calibration curve. Based on these data, the LOD of MX was calculated to be 0.3786 μg/ml ($n = 4$). The LOQ of MX was evaluated to be 1.147 μg/ml ($n = 4$).

2.2.11. In vitro dissolution test

Currently, there are no regulatory requirements or established protocols for *in vitro* dissolution testing of inhaled products (Riley et al., 2012; Radivojev et al., 2019). A modified paddle method (Hanson SR8 Plus, Teledyne Hanson Research, Chatsworth, CA, United States of America) from the European Pharmacopeia (European Pharmacopoeia 10.0, 2019)was used to define the release of MX from the solid dosage form. The applied samples contained 1.5 mg of MX, which is the tenth of the highest oral dose of MX (Meloxicam Pubchem). This is the estimated dose of MX for pulmonary delivery. There is no optimal method to determine the exact volume of the lung lining fluid. The estimated value is between 10 and 70 ml (Fröhlich et al., 2016). Considering the limitation of the dissolution setup, 50 ml of the previously mentioned (Section 2.2.10) simulated lung medium was applied during the measurement (Tay et al., 2018; Parlati, 2008). The paddle was rotated at 100 rpm to continuously homogenize the media. The measurement was performed up to 60 min at 37 °C (Pomázi, 2013). 5 ml of the samples were taken out after 5, 10, 15, 30, and 60 min. The medium was replenished in every case. After filtration (pore size: 0.45 μm, Millex-HV syringe-driven filter unit, Millipore Corporation, Bedford, United States of America) the dissolved quantity of MX was determined spectrophotometrically at a wavelength of 362 nm (ATI-UNICAM UV/VIS Spectrophotometer, Cambridge, United Kingdom). The measurement was executed three times.

2.2.12. In vitro permeability test

A modified horizontal diffusion cell was used to investigate the *in vitro* permeability of the samples. The diffusion cells are a 3D printed unique construction developed and validated by the research team (Gieszinger et al., 2021). The method is suitable for the investigations of alternative drug delivery routes. It provides a solution to measure the permeability properties of the samples in small volume and real-time.

The set-up of the apparatus is shown in Fig. 1. 9 ml of simulated lung medium was used as the donor phase. As previously mentioned, the volume of the lung lining fluid is 10–70 ml (Fröhlich et al., 2016), which is divided into different lung generations, therefore 9 ml was the ideal choice to model the absorption in the alveolar region. 9 ml of phosphate buffer (pH=7.4) was the acceptor phase, simulating the circumstances of the lung epithelium. Between the two phases, a cellulose membrane (RC 55 WhatmanTM GE Healthcare Life Sciences, Buckinghamshire, United Kingdom) was applied, which was impregnated with isopropyl myristate. The pore size of the membrane was 0.5 μm, its thickness was 0.75 μm. The diffusion surface was 0.785 cm^2. The rotation of the stirring bar was set to 300 rpm. The magnetic stirring bars were moved by CS-DSD1 Digital Magnetic Stirrer (CS-Smartlab Devices Ltd., Kozármislény, Hungary). The equipment was thermostated by a water jacket with the help of a circulator. The temperature was 37 °C during the investigation, which is the usual temperature inside the human lung. The diffusion model ensures a homogeneous distribution of pulmonary dry powder formulations by the continuous stirring of the donor phase and maintenance of temperature throughout the experiment. Samples containing 1.5 mg of MX were investigated, similarly to the dissolution test. The design of the chambers was suitable for real-time analysis with an immersion probe input. The amount of the diffused API to the acceptor phase was determined at the wavelength of 362 nm, for 60 min with the help of the spectrophotometric sonda (FDP-7UV200-VAR, Avaspec-ULS2048-USB2, Avantes, Apeldoorn, The Netherlands). Three parallel measurements were performed with the formulations. In case of the method, the LOD of MX was evaluated to be 0.7987 μg/ml ($n = 4$). The LOQ of MX was calculated to be 2.421 μg/ml ($n = 4$).

The flux (J) [μg/cm2/h] of MX was calculated from the quantity of MX, which permeated through the membrane, divided by the surface of the membrane insert and the duration time (Eq. (1)):

$$J = \frac{m}{A * t} \quad (1)$$

The permeability coefficient (Kp) [cm/h] was determined as a ratio of flux and the MX concentration in the donor phase [μg/cm3] (Eq. (2).):

$$Kp = \frac{J}{Cd} \quad (2)$$

2.2.13. *In vitro aerodynamic measurements*

The aerosolization properties of the nano spray-dried formulations were assessed *in vitro*, using an Andersen Cascade Impactor (ACI), (Apparatus D, Copley Scientific Ltd., Nottingham, United Kingdom) (European Pharmacopoeia 10.0, 2019) . The inhalation flow rate was set to 60 l/min (High-capacity Pump Model HCP5, Critical Flow Controller Model TPK, Copley Scientific Ltd., Nottingham, UK). The actual flow rate through the impactor was measured by a mass flow meter (Flow Meter Model DFM 2000, Copley Scientific Ltd., Nottingham, UK). The inhalation time was 4 s. The setting models the normal breathing pattern with a 4 l inhalation volume. Breezhaler®'s single-dose devices (Novartis International AG, Basel, Switzerland) were applied, with transparent, size 3 gelatine capsules (Capsugel, Bornem, Belgium) filled with the different powders. Between 2 and 3 mg of the dry samples were applied, therefore each capsule contained approximately 1.5 mg of the active ingredient. Four capsules were inhaled twice during one measurement. To simulate the pulmonary adhesive circumstances, the collection plates on the stages were coated with Span 85 and cyclohexane (1 + 99 w/w%) mixture. After inhalation, the device, the capsules, the induction port, the plates, and the filter were washed with methanol and pH 7.4 phosphate buffer (60+40 V/V%) to collect and dissolve the deposited amount of MX. The API was quantified by UV/Vis spectrophotometry (ATI-UNICAM UV/VIS Spectrophotometer, Cambridge, United Kingdom) at a wavelength of 362 nm. The *in vitro* aerodynamic properties were evaluated with the help of Inhalytix™ (Copley Scientific LTD., Nottingham, United Kingdom) data analysis software, which is a fully compliant, and validated aerodynamic particle size distribution data analysis solution. Fine particle fraction (FPF) and median mass aerodynamic diameter (MMAD) is the most widely used values. FPF is defined as the percentage of the mass of the active ingredient consisting of particles with an aerodynamic diameter of fewer than 5 μm divided by the emitted dose of the formulations. MMAD is influenced by the inhalation flow rate, density, size, and shape of the particle. The emitted fraction (EF) was also calculated, which is the released fraction from the DPI device.

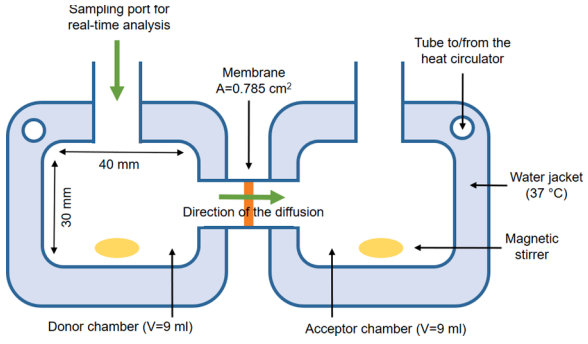

Fig. 1. The schematic set-up of the horizontal diffusion cells.

2.2.14. *Aerodynamic particle counter*

The drug products were loaded into capsules and a Breezhaler® (Novartis International AG, Basel, Switzerland) dry powder inhalator device was used for the tests in the measurement setup shown in Fig. 2. The measurement setup consists of a breath simulator, an induction port representing the upper respiratory tract, a vacuum pump with a critical flow controller, and an Aerodynamic Particle Sizer (APS). A constant airflow Q2 was established in the system along the blue arrows using the

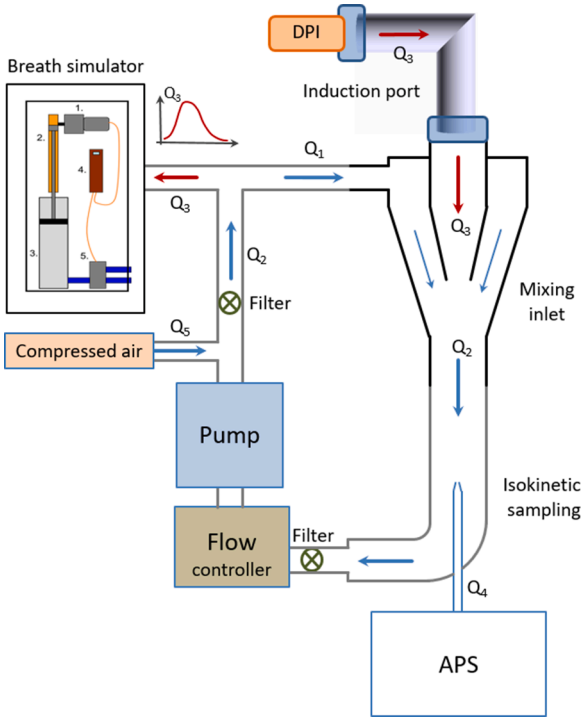

Fig. 2. The schematic design and components of the measurement setup: DPI, induction port, APS, vacuum pump with a critical flow controller, mixing inlet, and PWG. The pulmonary waveform generator consists of: 1-Servo motor; 2-Timing belt; 3-Piston pump; 4-PLC; 5-Valves (For interpretation of the references to color in this figure, the reader is referred to the web version of this article.).

pump (HCP5 High capacity pump; Copley Scientific Ltd., Nottingham, United Kingdom) and flow controller (TPK 2000; Copley Scientific Ltd., Nottingham, United Kingdom). The compressor compensates for the Q4 airflow taken by the particle counter and any losses. The airflow Q5 provided by the compressor was determined by measuring the airflow through the upper inlet of the mixing unit, in the inhaler side, in the default condition. During the measurements, the breathing simulator produced the flow profile Q3 activating the DPI unit through the mixing inlet (red arrows). The mixing inlet (Copley Scientific Ltd., Nottingham, United Kingdom) provides an interface between the flow that activates the DPI and the main stream that transfers the particles to the APS. The APS samples particles from the main stream by an isokinetic nozzle. A TSI 3321 (TSI Incorporated, Shoreview, Minnesota, United States of America) aerodynamic particle sizer was used for the measurements. The instrument measures the number size distributions of aerosol particles with aerodynamic diameters from 0.5 to 20 μm, in 52 channels. The instrument determines the aerodynamic size of the particles by time-of-flight measurement in an accelerated flow. The sample flow rate of the APS was 1 l/min and the sampling time was set to 5 s with no pause. Considering the length of the applied inhalation profile and the residence time of the particles in the measurement system the sampling time was set to 5 s during our investigations. As a breath simulator, we used an in-house developed pulmonary waveform generator. It uses a Piston pump driven by a PLC-controlled servo motor to generate the inhalation and exhalation air flows. The inhalation volume span from 0.1 cm3 to 6800 cm^3. The time resolution of the inhalation profile can be set to 20, 50, and 100 ms. For the measurements, the inhalation waveform programmed into the breathing simulator was constructed based on literature data (Abadelah et al., 2019; Farkas et al., 2019). The flow controller was used to set a flow rate of 90 l/min, which was regularly checked during the measurements with a TSI 4000 thermal mass flow meter (TSI Incorporated, Shoreview, Minnesota, United States of America), which measuring range is 0.5–200 Nl/min.

2.2.15. Cytotoxicity measurement

Before the cell line investigation, the spray-dried samples were dissolved in dimethyl sulphoxide (DMSO) (VWR Chemicals, Leuven, Belgium). During the measurements, a concentration of 0.1 mg/ml was applied. This concentration of MX is adequate for pulmonary delivery, for 1.5 mg of drug dose in approximately 15 ml of lung fluid volume (Fröhlich et al., 2016). Diluted samples were also measured for further investigation. A concentration of 0.05 and 0.025 mg/ml were tested. Mitochondrial activity as a measure of cell viability was performed by MTT (3-(4,5-dimethylthiazol-2-yl)−2,5-diphenyltetrazolium bromide) assay in 96-well cell culture microplates using A549 (adenocarcinomic human alveolar basal epithelial cells) (ATCC). A549 cells were seeded at a density of 4 × 104 cells/well. The cells were treated with either MX or nano[MX1_PVA_LEU0] or nano[MX1_PVA_LEU0.5] or nano [MX1_PVA_LEU1]. The maximum concentration of the tested compounds was 0.1 mg/ml. Furthermore, 5 μg/ml lipopolysaccharide (LPS; ThermoFisher Scientific Waltham, MA, USA) cytotoxicity was also measured. LPS was used to induce inflammation in the cells during the anti-inflammatory effect investigations (Crestani et al., 1994), therefore its cytotoxic effect was also tested (Section 2.2.16). Cells were incubated at 37 °C for 48 h. Later, 20 μl of thiazolyl blue tetrazolium bromide (Sigma, St. Louis, Missouri, USA) was added to each well. After additional incubation at 37 °C for 4 h, sodium dodecyl sulfate (Sigma, St. Louis, Missouri, USA) solution (10% in 0.01 M HCl) was added and incubated overnight. Cytotoxicity was then determined by measuring the OD at 550 nm (ref. 630 nm) with EZ READ 400 ELISA reader (Biochrom, Cambridge, United Kingdom). The assay was replicated four times for each concentration (Virók et al., 2017). Cell viability was concluded based on the following formula: $100 - ((OD_{sample} - OD_{medium\ control})/(ODc_{ell\ control} - OD_{medium\ control})) \times 100$.

2.2.16. Anti-inflammatory effect

The cells were propagated in minimum essential medium Eagle with Earle's salt (Sigma, St. Louis, MO, USA), and were supplemented with 25 μg/ml gentamycin, 10% foetal calf serum, 0.5% wt/vol glucose, 0.3 mg/ml l-glutamine and 4 nm HEPES. A549 cells were seeded in 6-well plates at a density of 1 × 106 cells/well and treated with 0.1 mg/ml of MX and 5 μg/ml of LPS or 0.1 mg/ml of nano[MX1_PVA_LEU0] and 5 μg/ml of LPS or 0.1 mg/ml of nano[MX1_PVA_LEU0.5] and 5 μg/ml of LPS or 0.1 mg/ml of nano[MX1_PVA_LEU1] and 5 μg/ml of LPS or 5 μg/ml of LPS or left untreated, then the cells were incubated for 48 h at 37 °C.

Total RNA extraction and cDNA synthesis. After 48 h of treatment, RNA was extracted using the TRI reagent (Sigma-Aldrich, St. Louis, Missouri, USA) according to the manufacturer's protocol. Subsequently, 0.1 μg of mRNA was reverse transcribed using Maxima Reverse Transcriptase according to the manufacturer's instructions using oligo(dT) primers (Thermo Fisher Scientific, Waltham, Massachusetts, USA).

qPCR amplification of IL-6, Actb. qPCR was performed using a Bio-Rad CFX96 real-time system with the 5x HOT FIREPol® EvaGreen® qPCR Supermix (Solis BioDyne, Tartu, Estonia) and the following human-specific primer pairs: IL-6: 5′-CAGCTATGAACTCCTTCTCCAC-3′, and 5′-GCGGCTACATCTTTGGAATCT −3′; Actb: 5′-TTCTACAATGAGCTGCGTGTGGCT-3′, and 5′-TAGCACAGCCTGGATAGCAACGTA −3′ Primers were designed using the Primer Quest Tool software and synthesized by Integrated DNA Technologies Inc. (Montreal, Quebec, Canada). Melting curve analysis was performed to verify amplification specificity. Threshold cycles (Ct) were determined for IL-6 and Actb, and the relative gene expression was calculated via the 2-(ΔΔCt) method. One-way analysis of variance with repeated measures (ANOVA RM) and planned comparisons was used to compare statistical differences in log2(ΔΔCt) values between infected and control samples, as described previously, with a level of significance of $P < 0.05$ (Hellemans et al., 2008).

Enzyme-linked immunosorbent assay (ELISA). After 48 h of treatment, the supernatant of the cells was collected and a standard sandwich human IL-6 ELISA kits Legend Max™ (BioLegend, San Diego, California, USA) was used to determine the IL-6 concentration. The supernatant of LPS-treated cells was diluted 10x. The assay was performed according to the manufacturer's instructions. The dynamic range of the kit was between 7.8 and 500 pg/ml. Plates were analyzed using the Biochrom Anthos 2010 microplate reader (Biochrom, Cambridge, United Kingdom). Samples were assayed in duplicate.

2.2.17. Statistical analysis

All described data indicate ± SD of three parallel measurements ($n = 3$). Statistical analysis was performed by one-way analysis of variance (ANOVA) using GraphPad Prism 8.0.1. software (GraphPad Software, CA, United States of America). *P*-values < 0.05 indicated statistically significant differences.

3. Results and discussion

3.1. Laser diffraction

The initial diameter of the API was in the micrometric size range (D [0.5]= 9.913 ± 0.371 μm), which successfully reached the nano range (Table 2). As a result of wet milling, the particle size of MX in the diluted suspension decreased to D[0.5]=137.70 nm ± 4.965 nm. SSA was increased from 1.09 ± 0.028 m2/g up to 43.65 ± 5.318 m2/g. Size reduction and higher surface area of the nanoparticles as compared to the microparticles will lead to a higher rate of dissolution (Dubey, 2006). After nano spray-drying, the D[0.5] values of the samples were

Table 2
Particle size of the API, the suspension, and the nano spray-dried samples. Data are means ± SD ($n = 3$ independent measurements).

Sample name	D[0.1] (μm)	D[0.5] (μm)	D[0.9] (μm)	Span	SSA (m^2/g)
MX	2.719 ± 0.057	9.913 ± 0.371	29.49 ± 0.630	2.70 ± 0.043	1.09 ± 0.028
suspension[MX_PVA]	0.067 ± 0.001	0.138 ± 0.005	0.555 ± 0.310	3.584 ± 2.056	43.65 ± 5.318
nano[MX1_PVA_LEU0]	0.441 ± 0.004	1.168 ± 0.004	6.770 ± 1.722	5.422 ± 1.488	6.600 ± 0.028
nano[MX1_PVA_LEU0.5]	0.659 ± 0.017	1.307 ± 0.036	2.854 ± 0.430	1.677 ± 0.296	5.185 ± 0.064
nano[MX1_PVA_LEU1]	0.789 ± 0.017	1.429 ± 0.088	3.400 ± 0.503	1.586 ± 0.116	4.385 ± 0.007

between 1 and 1.5 μm. The result was correlated to our initial aim, which was to produce particles below 2 μm. The geometric diameter of spray-dried MX1_PVA_LEU0 was around 1.17 μm. Incorporating LEU, the geometric size of the spray-dried particles increased, which led to a decreasing SSA. The reason is that the particle–particle interaction forces alter the particle diameter (Mangal et al., 2015). The distribution was monodisperse in the case of LEU-containing products (Span < 2.0), which is important for accurate dosing (Chvatal et al., 2017).

3.2. Dynamic light scattering

During DLS investigations the average diameters of the diluted suspension and the dispersed powders were measured (Table 3). The test showed that the particle diameter of the suspension was 359.75 ± 12 nm. The DLS results are more accurate than the laser diffraction in the nano range (Powers et al., 2007). In addition, we managed to reduce the diameter of the MX to under 500 nm. Therefore they can avoid the uptake by the alveolar macrophages (Thorley and Tetley, 2013). The average diameter of the dispersed spray-dried products was between 5 and 800 nm. This size results predict the behavior of the particles after deposition and disintegration in the airways. The polydispersity index (PdI) values correlated with the Span values of laser diffraction. It decreased when more LEU was added. The zeta potentials of the samples ranged between −21 and −25 mV, which demonstrated that our samples constituted a stable suspension system (Salopek et al., 1992). Systems with negative zeta potential are more degradable in the lung, therefore do not cause further infection or fibrosis due to long retention (Dailey et al., 2003).

3.3. Surface tension

Considering surface tension, a variable lowering of the surface tension of water at 25 °C (71.99 ± 0.36 mN/m) (Vargaftik et al., 1983), can be seen for the initial polymeric stabilizer. The surface tension of the 2.5% (w/V) PVA solution was 51.78 ± 1.315 mN/M. The surface tension value of the nanosuspension was grown to 66.07 ± 0.543 mN/M. Adding LEU could further increase the surface tension of the suspension (Gliński et al., 2000). The energy used by the mill to achieve particle size reduction can be defined as the collision energy. The collision energy is the sum of the kinetic energy of the beads acting perpendicular to the direction of the disk rotation and the collision heat generated by the milling components and the container wall (Bartos, 2016, 2019); . That energy introduced during the particle size reduction process leads to an increase in surface tension of the suspension, which is associated with the increase in the dissolution pressure. The change in the surface tension can also lead to increased saturation solubility (Muller et al., 1999).

Table 3
Average particle size, polydispersity index, and zeta potential of the suspension and the spray-dried products. Data are means ± SD ($n = 3$ independent measurements).

Sample name	D (nm)	PdI	Zeta potential (mV)
suspension[MX_PVA]	359.75 ± 12	0.340 ± 0.057	−23.70 ± 0.85
nano[MX1_PVA_LEU0]	676.70 ± 47	0.543 ± 0.055	−21.35 ± 5.27
nano[MX1_PVA_LEU0.5]	743.25 ± 27	0.502 ± 0.074	−23.30 ± 2.74
nano[MX1_PVA_LEU1]	526.90 ± 20	0.381 ± 0.031	−24.50 ± 1.47

However, a higher surface tension leads to a faster flow rate during nano spray-drying. Hence, a faster portion of fluid volume is delivered during the mesh vibration, leading to the formation of larger droplets (Arpagaus et al., 2017).

3.4. Scanning electron microscopy

According to the morphology investigation of the particles, a nearly spherical shape was observable (Fig. 3), which was due to the optimized nano spray-drying (Arpagaus et al., 2018). The particle diameter was measured based on the SEM pictures with the help of the Image-J program. The diameters were 692 ± 157 nm of nano[MX1_PVA_LEU0], 838 ± 307 of nano[MX1_PVA_LEU0.5] and 884 ± 198 nm of nano [MX1_PVA_LEU1]. Data are means ± SD ($n = 100$ independent measurements). The size results were correlated with the results of the previous particle size investigations. PVA prevented the aggregation of the particles, it makes a layer around the drug particles. This hydrophilic coat will also help the dissolution process of the API. Smooth surfaces are not preferred for pulmonary delivery since they tend to increase the interaction between particles while rough or wrinkled surfaces tend to increase the aerosolization efficiency. Changes in surface corrugation improve dispersibility by reducing contact points between particles, therefore achieving more separated particles. When LEU was present in the systems, preferable wrinkled, donut-like particles were established. Overall, the particles were forecasting a proper powder dispersion during inhalation, therefore higher drug delivery into the deeper regions of the lung (Sou et al., 2013; Chvatal et al., 2019; Party et al., 2021; Das et al., 2021).

3.5. X-ray powder diffraction

The XRPD pattern of the raw materials demonstrated, that MX and LEU had a crystalline structure. The presence of PVA did not affect the diffractograms, cause it had no crystalline properties. In the case of the products, the intensities of the characteristic peaks decreased (Fig. 4). Overall the wet milling and nano spray-drying procedures decreased crystallinity, which was determined via the mean of the decrease of the total area beneath the curve of the characteristic peaks compared with the physical mixtures. In nano[MX1_PVA_LEU0], nano[MX1_PVA_LEU0.5] and nano[MX1_PVA_LEU1] 68.19%, 66.11% and 54.04% of MX became amorphous, respectively (Bartos et al., 2016).

3.6. Differential scanning calorimetry

DSC was applied to determine the melting of PVA, LEU, and MX in the raw form, in the physical mixtures, and in the products (Fig. 5.). PVA had no endothermic peak. LEU had an endothermic peak at 294.41 °C, MX showed a sharper peak at 264.03 °C, reflecting its melting point and crystalline structure. After the preparation method, the DSC curves showed broader endothermic peaks of MX, indicating a decrease in its crystallinity. The MX crystals remaining in the samples melted at a lower temperature than the crystals of raw MX because of particle size reduction. This was helped by PVA, which has the glass transition temperature (Tg) value at 85 °C (Bartos et al., 2018).

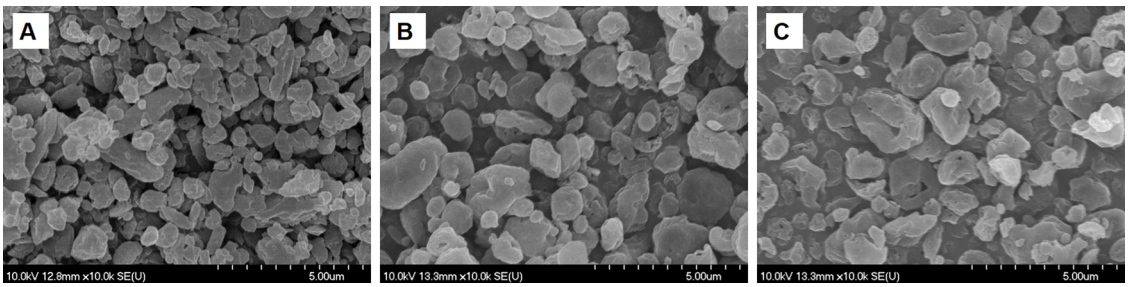

Fig. 3. SEM pictures of the spray-dried samples: A: nano[MX1_PVA_LEU0], B: nano[MX1_PVA_LEU0.5], C: nano[MX1_PVA_LEU1].

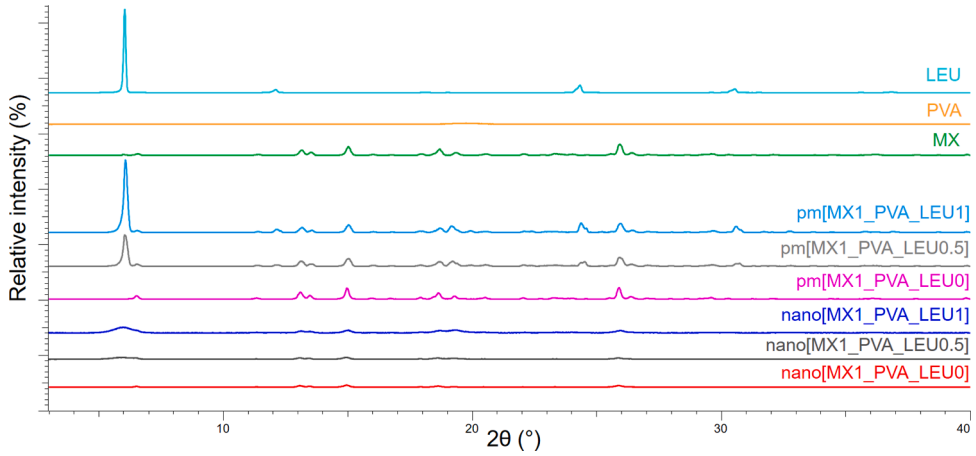

Fig. 4. XRPD results of the raw materials, (PVA, LEU, and MX), the physical mixtures (pm[MX1_PVA_LEU0], pm[MX1_PVA_LEU0.5], and pm[MX1_PVA_LEU1]), and the nano spray-dried samples (nano[MX1_PVA_LEU0], nano[MX1_PVA_LEU0.5], and nano[MX1_PVA_LEU1]).

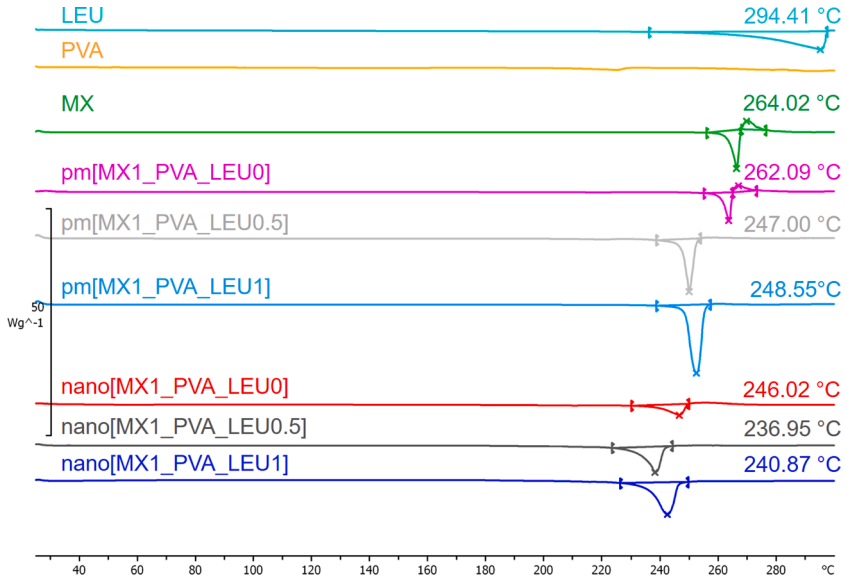

Fig. 5. DSC curves of the raw materials, (PVA, LEU, and MX), the physical mixtures (pm[MX1_PVA_LEU0], pm[MX1_PVA_LEU0.5], and pm[MX1_PVA_LEU1]), and the nano spray-dried samples (nano[MX1_PVA_LEU0], nano[MX1_PVA_LEU0.5], and nano[MX1_PVA_LEU1]).

3.7. Solubility test

The initial solubility of the raw MX was 0.502 ± 0.002 mg/ml in artificial lung media. As a result of the increased surface area of MX, the aqueous solubility of the nano spray-dried samples improved significantly in each case (Table 4 and Fig. 6). The reduction in the drug particle size in the nanometer range led to an increase in solubility, which predicted better dissolution properties. Both are significant factors to enhance the bioavailability of poorly water-soluble drugs (Böhm and Müller, 1999). Amorphous pharmaceuticals are markedly more soluble, than crystalline forms. Our investigations also confirmed, even partially amorphous features can significantly increase the solubility (Hancock and Parks, 2000)

Table 4
Solubility results of the initial drug and the spray-dried products. Data are means ± SD ($n = 3$ independent measurements).

Sample name	Solubility (mg/ml)
MX	0.905 ± 0.005
nano[MX1_PVA_LEU0]	2.025 ± 0.062
nano[MX1_PVA_LEU0.5]	1.501 ± 0.002
nano[MX1_PVA_LEU1]	1.581 ± 0.029

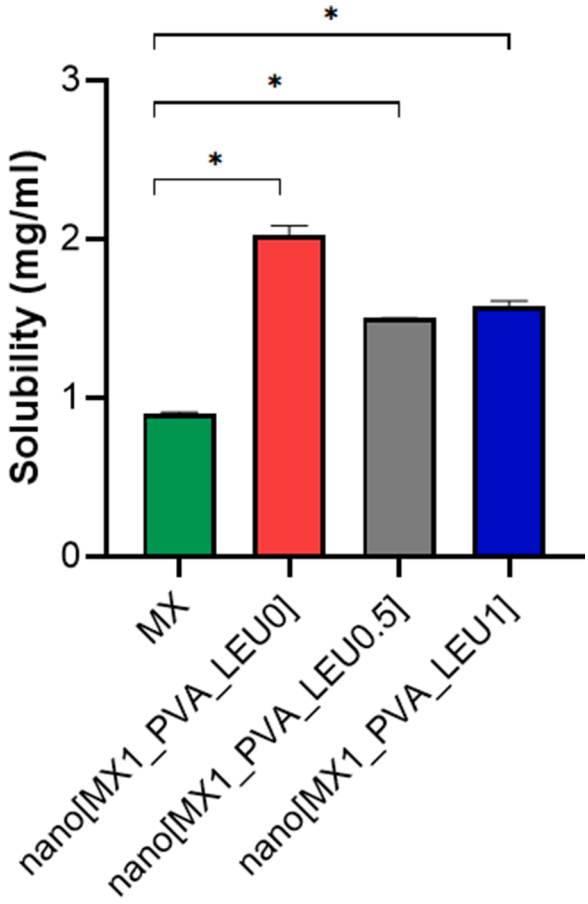

Fig. 6. Solubility results of the initial drug (MX), and the prepared samples (nano[MX1_PVA_LEU0], nano[MX1_PVA_LEU0.5], and nano[MX1_PVA_LEU1]). Data are means ± SD ($n = 3$ independent measurements). Level of significance: *$p < 0.05$).

3.8. *In vitro* dissolution

The results of the dissolution test confirmed our predictions. The released amount of MX was the lowest for the samples containing raw materials because of the poor water solubility of MX (Fig. 7). In the first 5 min, 47.04 ± 11.55% of the MX was released from the nano [MX1_PVA_LEU0], 71.82 ± 1 2.04% from the nano[MX1_PVA_LEU0.5], and 71.31±6.91% from the nano[MX1_PVA_LEU1]. All amount of the drug was released within an hour. The nano spray-dried samples showed significantly enhanced drug release compared to the physical mixtures (Fig. 8). These improvements could be related to the higher specific surface area, enhanced solubility, and the amorphization of the MX. The presence of PVA inhibited aggregation, and the use of LEU reduced the cohesion between the particles, therefore a larger amount of MX was liberated. The results of our formulations are advantageous in local therapy. The behavior of the particles gives enough time to release the nano-sized MX (Ruge et al., 2013). The sustained release can reduce the *in vivo* toxicity associated with the immediate burst release effect of the drug (Mukhtar et al., 2020).

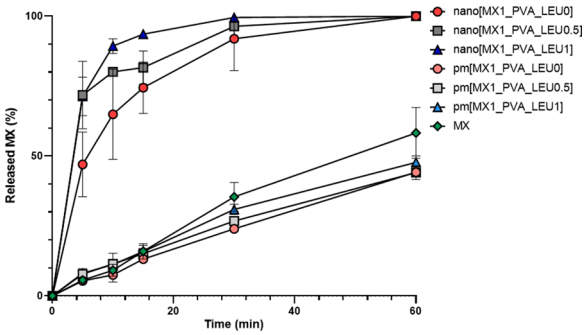

Fig. 7. *In vitro* dissolution results of the active ingredient (MX), the physical mixtures (pmMX1_PVA_LEU0, pmMX1_PVA_LEU0.5, and pmMX1_PVA_LEU1), and the prepared samples (nano[MX1_PVA_LEU0], nano[MX1_PVA_LEU0.5], and nano [MX1_PVA_LEU1]). Data are means ± SD ($n = 3$ independent measurements).

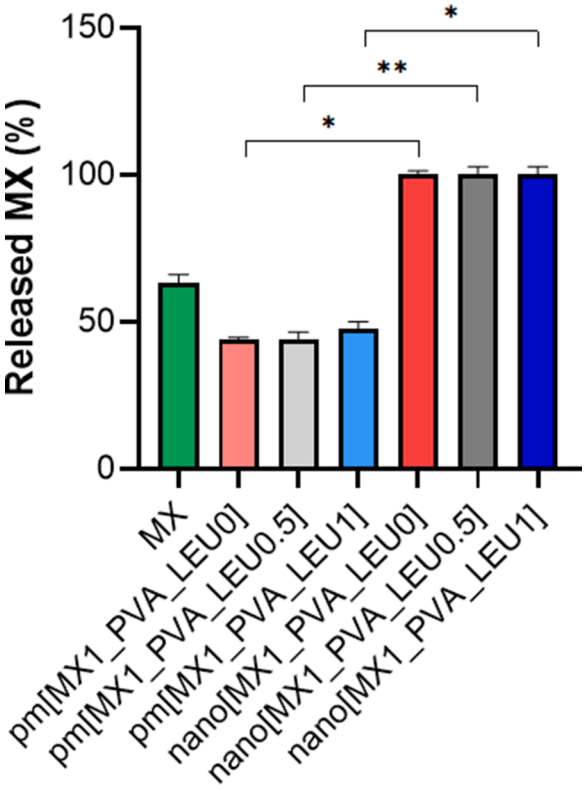

Fig. 8. *In vitro* dissolution results of the active ingredient (MX), the physical mixtures (pmMX1_PVA_LEU0, pmMX1_PVA_LEU0.5, and pmMX1_PVA_LEU1), compared to the spray-dried samples (nano[MX1_PVA_LEU0], nano [MX1_PVA_LEU0.5], and nano[MX1_PVA_LEU1]). Data are means ± SD ($n = 3$ independent measurements). Level of significance: *$p < 0.05$), **$p < 0.01$).

3.9. *In vitro* permeability

During the permeability investigations, the high surface area provided by the nano-sized particles was the main factor affecting the rate of passive diffusion. Diffusion from the nano spray-dried samples reached higher values than from raw materials (Fig. 9). These results were a remarkably high amount (85–110 μg/cm^2) if we take into consideration that the total surface of the lung is around 100 m^2 (Das and Stewart, 2016). The products showed a significantly increased flux (J) and permeability coefficient (Kp) compared with the raw materials

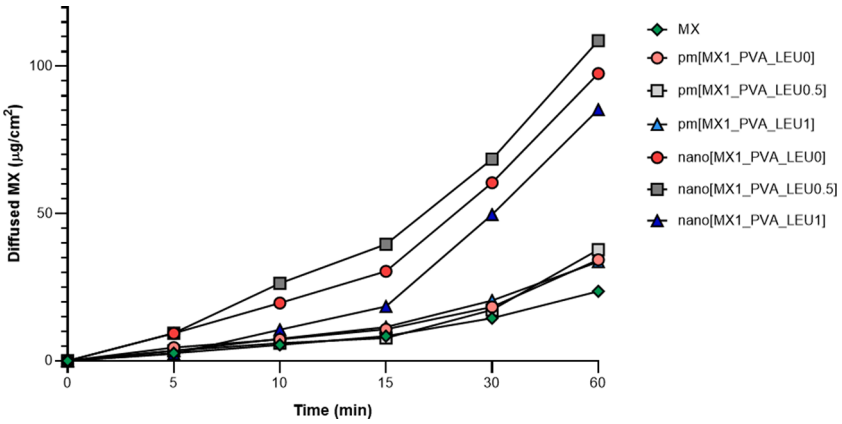

Fig. 9. *In vitro* permeability results of meloxicam (MX), the physical mixtures (pmMX1_PVA_LEU0, pmMX1_PVA_LEU0.5, and pmMX1_PVA_LEU1), and the prepared samples (nanoMX1_PVA_LEU0, nanoMX1_PVA_LEU0.5, and nanoMX1_PVA_LEU1). Data are means ± SD ($n = 3$ independent measurements).

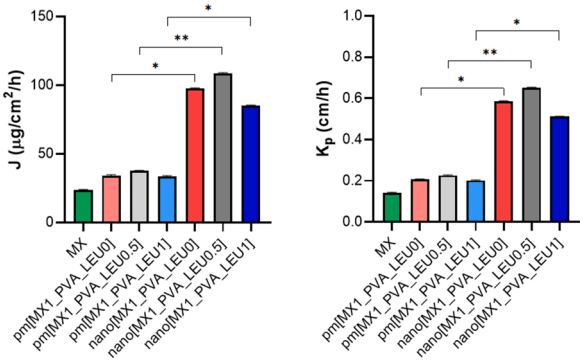

Fig. 10. The flux (J) and the permeability coefficient (K_p) results of meloxicam (MX), the physical mixtures (pmMX1_PVA_LEU0, pmMX1_PVA_LEU0.5, and pmMX1_PVA_LEU1), compared to the spray-dired samples (nanoMX1_PVA_LEU0, nanoMX1_PVA_LEU0.5, and nanoMX1_PVA_LEU1). Data are means ± SD ($n = 3$ independent measurements). Level of significance: *$p < 0.05$, **$p < 0.01$).).

(Fig. 10). Therefore, an enhanced amount of API could get into the epithelium with the nano spray-dried formulations.

3.10. *In vitro* aerodynamic results

The distribution of the initial drug and the products were determined during the aerodynamic assessment. The deposition of the samples on different parts of the set was shown in Fig. 11. An insufficient quantity of raw MX reached the stages of the impactor. The drug remained in the capsule and a high amount was deposited on the induction port. The nanoMX1_LEU0 sample also mostly stayed in the capsule, but it reached the third and fourth stages. Those plates demonstrated the bronchial area. A small amount of the product reached the filter. The application of LEU improved the aerosolization of the products owing to the reduced cohesion between the particles. LEU-containing samples were liberated from the capsule in a larger amount, compared to the LEU-free products. Besides the deposition on the third and fourth stages, the largest amount reached the filter, which represented the alveolar region. The calculated *in vitro* aerodynamic results by Inhalytix™ software were presented in Table 5. The results of nanoMX1_LEU0.5 and nanoMX1_LEU1 are preferential. The MMAD values were between 1.2 and 1.3 μm. These extra-fine particles could target the deeper airways (Usmani et al., 2005). The samples had outstanding FPF results between 87 and 95%. which is

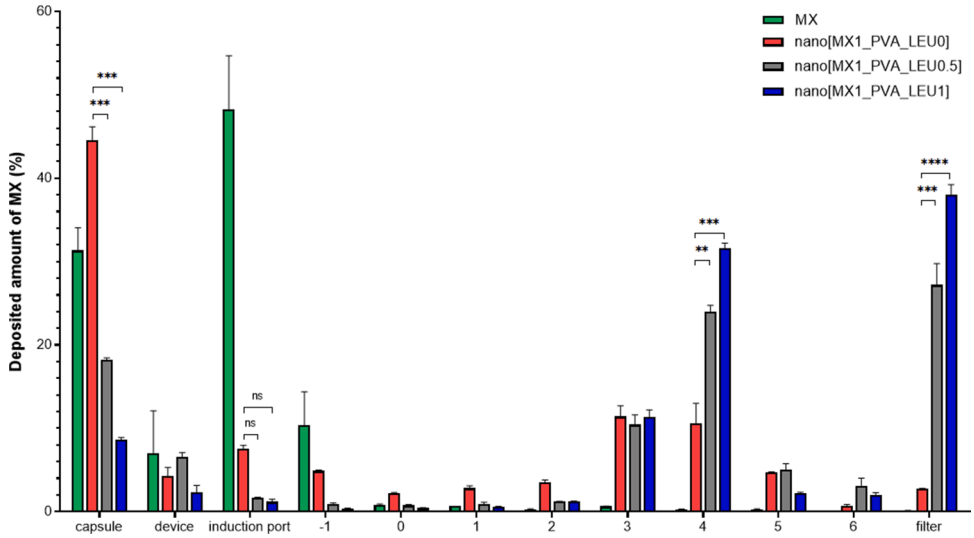

Fig. 11. *In vitro* aerodynamic distribution of the raw active ingredient and the gsamples at a flow rate of 60 l/min (MX, nano[MX1_PVA_LEU0], nano [MX1_PVA_LEU0.5], nano[MX1_PVA_LEU1]). Data are means ± SD ($n = 3$ independent measurements). Level of significance: ** $p < 0.01$, *** $p < 0.001$, **** $p < 0.0001$).

Table 5
In vitro aerodynamic properties: mass median aerodynamic diameter (MMAD), fine particle fraction (FPF), and emitted fraction (EF) of the spray-dried samples at a flow 60 L/min.). Data are means ± SD ($n = 3$ independent measurements).

Sample name	MMAD (μm)	FPF by size (%)	FPF by stage (%)	EF (%)
nano [MX1_PVA_LEU0]	2.151 ± 0.106	62.62 ± 0.201	65.93 ± 0.226	30.50 ± 1.131
nano [MX1_PVA_LEU0.5]	1.344 ± 0.231	86.16 ± 2.327	86.99 ± 2.086	58.77 ± 11.06
nano [MX1_PVA_LEU1]	1.265 ± 0.072	94.45± 0.883	94.91 ± 0.812	80.90 ± 10.97

larger than the FPF values of the commercially available Breezhaler® formulations (Chapman et al., 2011). The emitted fraction (EF) was also higher in the LEU-containing products, indicating a weaker adhesive character between the powder and the gelatine capsule.

3.11. Aerodynamic particle counter investigation

The best formulation (nano[MX1_PVA_LEU1) according to the ACI measurement was chosen for further aerodynamic characterization. Size results were determined based on the number, surface, and mass of the particles. The aerodynamic particles counter confirmed the particles' size between 1 and 1.4 μm (Table 6). These results also corresponded to the definition of extra-fine particles ($d < 2$ μm) (Hillyer et al., 2018), which was our initial goal.

3.12. Cytotoxicity measurement

Cytotoxicity studies represented that all the substances have a low cytotoxic effect in a concentration of 0.1 mg/ml. The cell viability was in order to MX, nano[MX1_PVA_LEU0], nano[MX1_PVA_LEU0.5], nano [MX1_PVA_LEU1] 91.97%, 90.32%, 80.38%, and 82.77%. The effect is not measurable at a concentration of 0.0125 mg/ml (Fig. 12). LPS had no cytotoxic effect at the highest concentration (data not shown). The results showed similarity to previous cytotoxicity effect investigations of MX (Ambrus et al., 2011; Chvatal et al., 2018; Varga et al., 2021). The formulations are safe for pulmonary administration. A549 cell lines exhibited similarities with type II. Alveolar epithelial cells, therefore the results are valid for imitating the circumstances of the small airways (Forbes, 2000).

3.13. Anti-inflammatory effect

Nano-sized MX solution inhibits IL-6 production on the translational level but not on the transcriptional level. LPS is a potent pro-inflammatory agent and increases IL-6 production in A549 cells (Crestani et al., 1994). LPS-treated cells showed significantly higher IL-6 relative expression compared to untreated cells (Fig. 13), however, neither MX solution nor nano-sized MX solutions inhibited the increase of IL-6 relative expression compared to LPS-treated cells (Fig. 14). Consequently, the IL-6 level was also checked via ELISA, and it was found that IL-6 expression increased significantly in LPS-treated cells

Table 6
The results of aerodynamic particle counting in case of nano[MX1_PVA_LEU1]. Data are means ± SD ($n = 4$ independent measurements).

	Number particle size	Surface particle size	Mass particle size
Median (μm)	0.989 ± 0.038	1.235 ± 0.044	1.355 ± 0.042
Mean (μm)	1.038 ± 0.035	1.268 ± 0.041	1.388 ± 0.038
Geometric Mean (μm)	0.986 ± 0.030	1.210 ± 0.039	1.330 ± 0.041
Mode (μm)	1.039 ± 0.059	1.290 ± 0.073	1.185 ± 0.466
Geometric Standard Deviation	1.378 ± 0.010	1.368 ± 0.017	1.355 ± 0.026

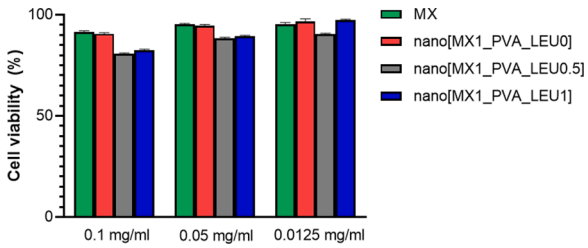

Fig. 12. Cell viability assay of substances on A549 cell line. A549 cells were treated with MX or nano[MX1_PVA_LEU0] or nano[MX1_PVA_LEU0.5] or nano [MX1_PVA_LEU1]. After an incubation period of 48 h, an MTT assay was performed to check the effect of the treatment on cell replication. Data are means ± SD ($n = 3$ independent measurements).

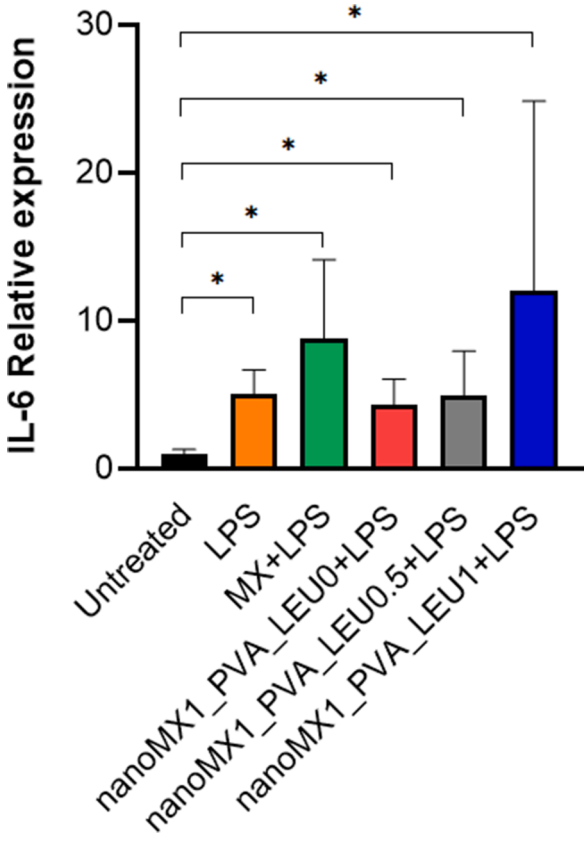

Fig. 13. Relative expression of IL-6. A549 cells were treated with 0.1 mg/ml nano[MX1_PVA_LEU0] and 5 μg/ml LPS or 0.1 mg/ml nano[MX1_PVA_LEU0.5] and 5 μg/ml LPS or 0.1 mg/ml nano[MX1_PVA_LEU1] and 5 μg/ml LPS or 0.1 mg/ml MX and 5 μg/ml LPS or 5 μg/ml LPS or left untreated. After 48 h, RNA was extracted from the cells and gene expression was analyzed for IL-6 via RT-qPCR. Bars denote the mean and standard deviation of the expression level for triplicate measurements. Level of significance: $*p < 0.05$).

compared to untreated cells. Interestingly, MX solution and all of the nano-sized MX impeded IL-6 production (Fig. 10). IL-6 is a biomarker and a potential therapeutic target for patients infected with COVID-19. An increase in proinflammatory cytokine IL-6 concentration correlates with respiratory failure, poor outcomes, and mortality in SARS-CoV-2. The reduction of this and other cytokines at an early stage is promising in regards to moderating immune responses in acute SARS-CoV-2 infection (Copaescu et al., 2020).

4. Conclusion

The purpose of our research work was to develop a carrier-free dry

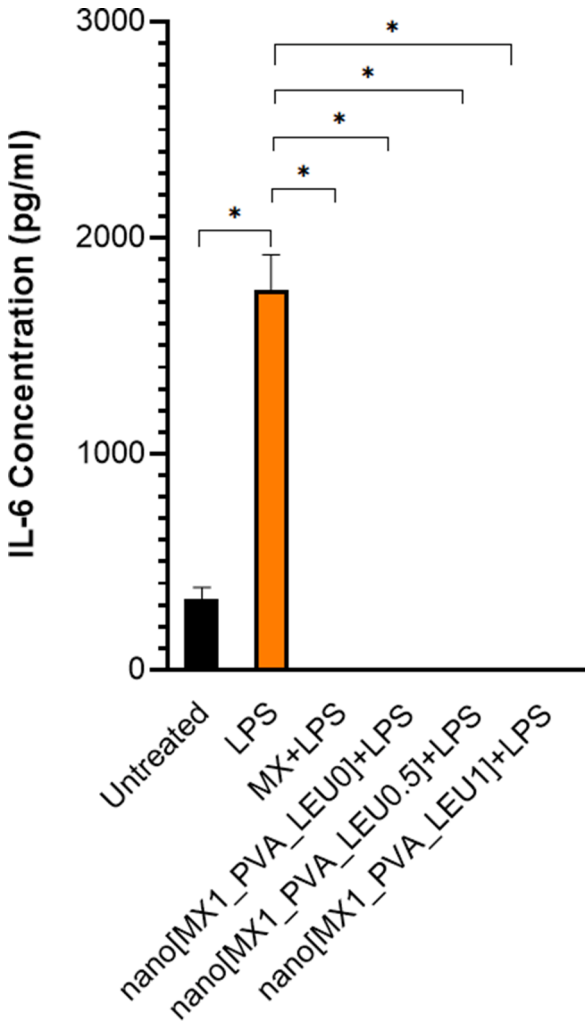

Fig. 14. Concentration of IL-6 in cell supernatants. Cells were treated with 0.1 mg/ml nano[MX1_PVA_LEU0] and 5 μg/ml LPS or 0.1 mg/ml nano [MX1_PVA_LEU0.5] and 5 μg/ml LPS or 0.1 mg/ml nano[MX1_PVA_LEU1] and 5 μg/ml LPS or 0.1 mg/ml MX and 5 μg/ml LPS or 5 μg/ml LPS or left untreated for 48 h. IL-6 concentration was measured via ELISA. Each bar denotes the mean standard deviation for triplicate measurements. Level of significance: *$p < 0.05$).

powder inhaler system combining the advantages of a nano-sized active ingredient and inhalable extra-fine powders. The particle size of the API was successfully reduced by wet milling and resulted in a nano-suspension ($d = 138$ nm). Nano spray-dried extra-fine inhalable powders were prepared from the nanosuspension. The final dry samples contained MX, stabilizing additive (PVA), and aerosolization adjuvant (LEU). The particles showed nearly spherical morphology and diameter between 1 and 1.5 μm. The particle size of the powders was complied with the definition of extra-fine particles. More than half of MX was detected in an amorphous state according to the XRPD measurements. The DSC investigations also demonstrated partial amorphization. Thanks to the particle size reduction, the solubility increased to 1.5–2.0 mg/ml. *In vitro* dissolution improved in the artificial lung medium compared to the initial material. *In vitro* permeability of the samples also got larger (85–110 μg/cm^2/h). LEU-containing samples showed outstanding aerodynamic properties during the *in vitro* aerodynamic measurements: FPF around 90%, and MMAD around 1 μm. The aerodynamic particle counter method also proved the proper extra-fine particle size. The samples showed no cytotoxicity during the *in vitro* investigations and reduced the IL-6 concentration to zero. Based on the anti-inflammatory activities of meloxicam, the newly prepared nanosized MX containing extra-fine microcomposites might be used in the local treatment of alveolar inflammation. Our formulating study makes good grounds for further investigations of the *in vivo* effectiveness and potential therapeutical use of MX in pulmonary therapy.

Funding

This research was funded by the University of Szeged Open Access Fund Grant No. 5674.

CRediT authorship contribution statement

Petra Party: Conceptualization, Methodology, Investigation, Data curation, Writing – review & editing, Visualization. **Dávid Kókai:** Methodology, Investigation, Data curation, Writing – review & editing. **Katalin Burián:** Supervision. **Attila Nagy:** Methodology, Investigation, Data curation, Writing – review & editing. **Béla Hopp:** Methodology, Investigation, Data curation, Writing – review & editing. **Rita Ambrus:** Conceptualization, Methodology, Investigation, Project administration, Supervision.

Declaration of Competing Interest

None.

Acknowledgments

Project no. TKP2021-EGA-32 has been implemented with the support provided by the Ministry of Innovation and Technology of Hungary from the National Research, Development and Innovation Fund, financed under the TKP2021-EGA funding scheme. This work was supported by the GINOP-2.3.2–15–2016–00036, Richter-GINOP-2.2.1–15–2016–00007, and by Gedeon Richter's Talentum Foundation, Gedeon Richter Ltd.

References

Abadelah, M., Chrystyn, H., Larhrib, H., 2019. Use of inspiratory profiles from patients with chronic obstructive pulmonary disease (COPD) to investigate drug delivery uniformity and aerodynamic dose emission of indacaterol from a capsule based dry powder inhaler. Eur. J. Pharm. Sci. 134, 138–144. https://doi.org/10.1016/j.ejps.2019.04.018.

Alhajj, N., O'Reilly, N.J., Cathcart, H., 2021. Designing enhanced spray dried particles for inhalation: a review of the impact of excipients and processing parameters on particle properties. Powder Technol. 384, 313–331. https://doi.org/10.1016/j.powtec.2021.02.031.

Ambrus, R., Pomázi, A., Réti-Nagy, K., Fenyvesi, F., Vecsernyés, M., Szabó-Révész, P., 2011. Cytotoxicity testing of carrier-based microcomposites for DPI application. Pharmazie 66, 549–550. https://doi.org/10.1691/ph.2011.0378.

Arpagaus, C., Collenberg, A., Rütti, D., Assadpour, E., Jafari, S.M., 2018. Nano spray drying for encapsulation of pharmaceuticals. Int. J. Pharm. 546, 194–214. https://doi.org/10.1016/j.ijpharm.2018.05.037.

Arpagaus, C., John, P., Collenberg, A., Rütti, D., 2017. 10 - Nanocapsules formation By Nano Spray drying. Nanoencapsulation Technologies for the Food and Nutraceutical Industries. Elsevier Inc. https://doi.org/10.1016/B978-0-12-809436-5/00010-0.

Bartos, Csilla, 2016. Application of wet milling techniques to produce micronized and nanonized drug predispersion for the development of intranasal formulations. PhD Thesis.

Bartos, Csaba, 2019. Optimization of a combined wet milling process to produce nanosuspension and its transformation into surfactant-free solid compositions to increase the product stability and drug bioavailability. PhD Thesis.

Bartos, C., Jójárt-Laczkovich, O., Katona, G., Budai-Szűcs, M., Ambrus, R., Bocsik, A., Gróf, I., Deli, M.A., Szabó-Révész, P., 2018. Optimization of a combined wet milling process in order to produce poly(vinyl alcohol) stabilized nanosuspension. Drug Des. Dev. Ther. 12, 1567–1580. https://doi.org/10.2147/DDDT.S159965.

Bartos, C., Szabó-Révész, P., Bartos, C., Katona, G., Jójárt-Laczkovich, O., Ambrus, R., 2016. The effect of an optimized wet milling technology on the crystallinity, morphology and dissolution properties of micro- and nanonized meloxicam. Molecules 21. https://doi.org/10.3390/molecules21040507.

Benke, E., Farkas, Á., Szabó-Révész, P., Ambrus, R., 2020. Development of an innovative, carrier-based dry powder inhalation formulation containing spray-dried meloxicam potassium to improve the *in vitro* and *in silico* aerodynamic properties. Pharmaceutics 12, 1–19. https://doi.org/10.3390/pharmaceutics12060535.

Böhm, Bernhard H.L., Müller, Rainer H., 1999. Lab-scale production unit design for nanosuspensions of sparingly soluble cytotoxic drugs. Pharm. Sci. Technol. Today 2 (8), 336–339. https://doi.org/10.1016/S1461-5347(99)00177-7.

Chapman, K.R., Fogarty, C.M., Peckitt, C., Lassen, C., Jadayel, D., Dederichs, J., Dalvi, M., Kramer, B., 2011. Delivery characteristics and patients' handling of two single-dose dry-powder inhalers used in COPD. Int. J. COPD 6, 353–363. https://doi.org/10.2147/COPD.S18529.

Chen S, Jennifer, Alfajaro, Mia Madel, Wei, Jin, Chow, Ryan D., Filler, Renata B., Eisenbarth, Stephanie C., Wilen,, Craig B., 2020. Cyclooxgenase-2 is induced by SARS-CoV-2 infection but does not affect viral entry or replication. bioRxiv. https://doi.org/10.1101/2020.09.24.312769.

Chugh, H., Awasthi, A., Agarwal, Y., Gaur, R.K., Dhawan, G., Chandra, R., 2021. A comprehensive review on potential therapeutics interventions for COVID-19. Eur. J. Pharmacol. 890, 173741 https://doi.org/10.1016/j.ejphar.2020.173741.

Chvatal, A., Alzhrani, R., Tiwari, A.K., Ambrus, R., Szabó-Révész, P., Boddu, S.H.S., 2018. Cytotoxicity of inhalable dry powders in A549 human lung cancer cell line. Farmacia 66, 172–175.

Chvatal, A., Ambrus, R., Party, P., Katona, G., Jójárt-Laczkovich, O., Szabó-Révész, P., Fattal, E., Tsapis, N., 2019. Formulation and comparison of spray dried non-porous and large porous particles containing meloxicam for pulmonary drug delivery. Int. J. Pharm. 559, 68–75. https://doi.org/10.1016/j.ijpharm.2019.01.034.

Chvatal, A., Farkas, Á., Balásházy, I., Szabó-Révész, P., Ambrus, R., 2017. Aerodynamic properties and *in silico* deposition of meloxicam potassium incorporated in a carrier-free DPI pulmonary system. Int. J. Pharm. 520, 70–78. https://doi.org/10.1016/j.ijpharm.2017.01.070.

Copaescu, A., Smibert, O., Gibson, A., Phillips, E.J., Trubiano, J.A., 2020. The role of IL-6 and other mediators in the cytokine storm associated with SARS-CoV-2 infection. J. Allergy Clin. Immunol. 146, 518–534. https://doi.org/10.1016/j.jaci.2020.07.001 e1.

Crestani, B., Comillet, P., Dehoux, M., Rolland, C., Guenounou, M., Aubier, M., National, I., Sant, D., Medicale, R., A, O.L.D.B., Bichat, F.X., 1994. Alveolar type II epithelial cells produce interleukin-6 *in vitro* and *in vivo*. Regulation by alveolar macrophage secretory products. J. Clin. Investig. 94, 731–740.

Dailey, L.A., Kleemann, E., Wittmar, M., Gessler, T., Schmehl, T., Roberts, C., Seeger, W., Kissel, T., 2003. Surfactant-free, biodegradable nanoparticles for aerosol therapy based on the branched polyesters, DEAPA-PVAL-g-PLGA. Pharm. Res. 20, 2011–2020. https://doi.org/10.1023/B:PHAM.0000008051.94834.10.

Das, S.C., Khadka, P., Shah, R., McGill, S., Smyth, H.D.C., 2021. Nanomedicine in Pulmonary delivery. Theory and Applications of Nonparenteral Nanomedicines. Elsevier Inc. https://doi.org/10.1016/b978-0-12-820466-5.00014-4.

Das, S.C., Stewart, P.J., 2016. The influence of lung surfactant liquid crystalline nanostructures on respiratory drug delivery. Int. J. Pharm. 514, 465–474. https://doi.org/10.1016/j.ijpharm.2016.06.029.

De Boer, A.H., Gjaltema, D., Hagedoorn, P., Frijlink, H.W., 2015. Can "extrafine" dry powder aerosols improve lung deposition? Eur. J. Pharm. Biopharm. 96, 143–151. https://doi.org/10.1016/j.ejpb.2015.07.016.

Dubey, R., 2006. Impact of nanosuspension technology on drug discovery and development. Drug Deliv. Technol. 5, 67–71.

European Pharmacopoeia 10.0, 2019. 2.9.3. Dissolution test for solid dosage forms. European Pharmacopeia 10.0. EDQM Council of Europe.

European Pharmacopoeia 10.0, 2019. 2.9.18. Preparations for inhalation: aerodynamic assessment of fine particles. European Pharmacopoeia 10.0. EDQM Council of Europe.

Farkas, Á., Szipőcs, A., Horváth, A., Horváth, I., Gálffy, G., Varga, J., Galambos, K., Kugler, S., Nagy, A., Szalai, Z., 2019. Establishment of relationships between native and inhalation device specific spirometric parameters as a step towards patient tailored inhalation device selection. Respir. Med. 154, 133–140. https://doi.org/10.1016/j.rmed.2019.06.021.

Forbes, Ben, 2000. Human airway epithelial cell lines for in vitro drug transport and metabolism studies. Pharm. Sci. Technol. Today 3 (1).

Fröhlich, E., Mercuri, A., Wu, S., Salar-Behzadi, S., 2016. Measurements of deposition, lung surface area and lung fluid for simulation of inhaled compounds. Front. Pharmacol. 7, 1–10. https://doi.org/10.3389/fphar.2016.00181.

Gieszinger, P., Kiss, T., Szabó-Révész, P., Ambrus, R., 2021. The development of an *in vitro* horizontal diffusion cell to monitor nasal powder penetration inline. Pharmaceutics 13. https://doi.org/10.3390/pharmaceutics13060809.

Gliński, J., Chavepeyer, G., Platten, J.K., 2000. Surface properties of aqueous solutions of l-leucine. Biophys. Chem. 84, 99–103. https://doi.org/10.1016/S0301-4622(99)00150-7.

Hancock, B.C., Parks, M., 2000. What is the true solubility advantage for amorphous pharmaceuticals? Pharm. Res. 17, 397–404. https://doi.org/10.1023/A:1007516718048.

Hellemans, J., Mortier, G., De Paepe, A., Speleman, F., Vandesompele, J., 2008. qBase relative quantification framework and software for management and automated analysis of real-time quantitative PCR data. Genome Biol. 8 https://doi.org/10.1186/gb-2007-8-2-r19.

Heyder, J., 2004. Deposition of inhaled particles in the human respiratory tract and consequences for regional targeting in respiratory drug delivery. Proc. Am. Thorac. Soc. 1, 315–320. https://doi.org/10.1513/pats.200409-046TA.

Hillyer, E.V., Price, D.B., Chrystyn, H., Martin, R.J., Israel, E., van Aalderen, W.M.C., Papi, A., Usmani, O.S., Roche, N., 2018. Harmonizing the nomenclature for therapeutic aerosol particle size: a proposal. J. Aerosol Med. Pulm. Drug Deliv. 31, 111–113. https://doi.org/10.1089/jamp.2017.1396.

ICH Harmonised Tripartite Guideline, 2005. Validation of Analytical Procedures: Text and Methodology. ICH Harmonised Tripartite Guideline.

Iwabuchi, K., Yoshie, K., Kurakami, Y., Takahashi, K., Kato, Y., Morishima, T., 2020. Therapeutic potential of ciclesonide inahalation for COVID-19 pneumonia: report of three cases. J. Infect. Chemother. 26, 625–632. https://doi.org/10.1016/j.jiac.2020.04.007.

Jetzer, M.W., Morrical, B.D., Schneider, M., Edge, S., Imanidis, G., 2018. Probing the particulate microstructure of the aerodynamic particle size distribution of dry powder inhaler combination products. Int. J. Pharm. 538, 30–39. https://doi.org/10.1016/j.ijpharm.2017.12.046.

Keck, C.M., Müller, R.H., 2006. Drug nanocrystals of poorly soluble drugs produced by high pressure homogenisation. Eur. J. Pharm. Biopharm. 62, 3–16. https://doi.org/10.1016/j.ejpb.2005.05.009.

Li, Q., Rudolph, V., Weigl, B., Earl, A., 2004. Interparticle van der Waals force in powder flowability and compactibility. Int. J. Pharm. 280, 77–93. https://doi.org/10.1016/j.ijpharm.2004.05.001.

Li, X., Anton, N., Arpagaus, C., Belleteix, F., Vandamme, T.F., 2010. Nanoparticles by spray drying using innovative new technology: the Büchi nano spray dryer B-90. J. Control. Release 147, 304–310. https://doi.org/10.1016/j.jconrel.2010.07.113.

Madas, B.G., Füri, P., Farkas, Á., Nagy, A., Czitrovszky, A., Balásházy, I., Schay, G.G., Horváth, A., 2020. Deposition distribution of the new coronavirus (SARS-CoV-2) in the human airways upon exposure to cough-generated droplets and aerosol particles. Sci. Rep. 10, 1–8. https://doi.org/10.1038/s41598-020-79985-6.

Malamatari, M., Charisi, A., Malamataris, S., Kachrimanis, K., Nikolakakis, I., 2020. Spray drying for the preparation of nanoparticle-based drug formulations as dry powders for inhalation. Processes 8. https://doi.org/10.3390/pr8070788.

Mangal, S., Meiser, F., Tan, G., Gagenbach, T., Denman, J., Rowles, M.R., Larson, I., Morton, D.A.V, 2015. Relationship between surface concentration of L -leucine and bulk powder properties in spray dried formulations. Eur. J. Pharm. Biopharm. 1–10. https://doi.org/10.1016/j.ejpb.2015.04.035.

Mukhtar, M., Pallagi, E., Csóka, I., Benke, E., Farkas, Á., Zeeshan, M., Burián, K., Kókai, D., Ambrus, R., 2020. Aerodynamic properties and *in silico* deposition of isoniazid loaded chitosan/thiolated chitosan and hyaluronic acid hybrid nanoplex DPIs as a potential TB treatment. Int. J. Biol. Macromol. 165, 3007–3019. https://doi.org/10.1016/j.ijbiomac.2020.10.192.

Muralidharan, P., Malapit, M., Mallory, E., Hayes, D., Mansour, H.M., 2015. Inhalable nanoparticulate powders for respiratory delivery. Nanomed. Nanotechnol. Biol. Med. 11, 1189–1199. https://doi.org/10.1016/j.nano.2015.01.007.

Ong, S.W.X., Tan, W.Y.T., Chan, Y.H., Fong, S.W., Renia, L., Ng, L.F.P., Leo, Y.S., Lye, D. C., Young, B.E., 2020. Safety and potential efficacy of cyclooxygenase-2 inhibitors in coronavirus disease 2019. Clin. Transl. Immunol. 9, 1–9. https://doi.org/10.1002/cti2.1159.

Pallagi, E., Karimi, K., Ambrus, R., Szabó-Révész, P., Csóka, I., 2016. New aspects of developing a dry powder inhalation formulation applying the quality-by-design approach. Int. J. Pharm. 511, 151–160. https://doi.org/10.1016/j.ijpharm.2016.07.003.

Parlati, C., 2008. Respirable Microparticles of Aminoglycoside Antibiotics for Pulmonary Administration. University of Parma.

Party, P., Bartos, C., Farkas, Á., Szabó-révész, P., Ambrus, R., 2021. Formulation and *In vitro* and *in silico* characterization of " Nano-in-Micro " dry powder inhalers containing meloxicam. Pharmaceutics 13, 1–18. https://doi.org/10.3390/pharmaceutics13020211.

Pomázi, Anita, 2013. Meloxikám tartalmú hordozó-alapú porinhalációs rendszer fejlesztése és vizsgálata lokális hatás elérése céljából. PhD Thesis.

Pomázi, A., Buttini, F., Ambrus, R., Colombo, P., Szabó-Révész, P., 2013. Effect of polymers for aerolization properties of mannitol-based microcomposites containing meloxicam. Eur. Polym. J. 49, 2518–2527. https://doi.org/10.1016/j.eurpolymj.2013.03.017.

Potočnik, J., 2011. Commission recommendation of 18 October 2011 on the definition of nanomaterial. Off. J. Eur. Union. https://doi.org/10.7748/ns.24.26.6.s4.

Powers, K.W., Palazuelos, M., Moudgil, B.M., Roberts, S.M., 2007. Characterization of the size, shape, and state of dispersion of nanoparticles for toxicological studies. Nanotoxicology 1, 42–51. https://doi.org/10.1080/17435390701314902.

Prasad, Ayya Rajendra, Thireesha, Bannaravuri, 2018. UV-spectrophotometric method development and validation for the determination of lornoxicam in microsponges. Int. J. Appl. Pharm. 10 (1), 74–78. https://doi.org/10.22159/ijap.2018v10i1.22357.

Radivojev, S., Zellnitz, S., Paudel, A., Fröhlich, E., 2019. Searching for physiologically relevant *in vitro* dissolution techniques for orally inhaled drugs. Int. J. Pharm. 556, 45–56. https://doi.org/10.1016/j.ijpharm.2018.11.072.

R.H. Muller, R. Becker, B. Kruss, K. Peters, Berlin, all of, Germany, 1999. Pharmaceutical nanosuspensions for medcament administrationas systems with increased saturation solubility and rate of solution. United States Pat. 1–30.

Riley, T., Christopher, D., Arp, J., Casazza, A., Colombani, A., Cooper, A., Dey, M., Maas, J., Mitchell, J., Reiners, M., Sigari, N., Tougas, T., Lyapustina, S., 2012. Challenges with developing *in vitro* dissolution tests for orally inhaled products (OIPs). AAPS PharmSciTech 13, 978–989. https://doi.org/10.1208/s12249-012-9822-3.

Ruge, C.C., Kirch, J., Lehr, C.M., 2013. Pulmonary drug delivery: from generating aerosols to overcoming biological barriers-therapeutic possibilities and technological challenges. Lancet Respir. Med. 1, 402–413. https://doi.org/10.1016/S2213-2600(13)70072-9.

Salopek, Branko, Krasic, Dragan, Filipovic, Suzana, 1992. Measurement and application of zeta-potential. Rudarsko-geolosko-naftni zbornik 4, 147–151.

Sarcinelli, M.A., Martins da Silva, T., Artico Silva, A.D., Ferreira de Carvalho Patricio, B., Mendes de Paiva, F.C., Santos de Lima, R., Leal da Silva, M., Antunes Rocha, H.V., 2021. The pulmonary route as a way to drug repositioning in COVID-19 therapy. J. Drug Deliv. Sci. Technol. 63 https://doi.org/10.1016/j.jddst.2021.102430.

Scherließ, R., Bock, S., Bungert, N., Neustock, A., Valentin, L., 2022. Particle engineering in dry powders for inhalation. Eur. J. Pharm. Sci. 172 https://doi.org/10.1016/j.ejps.2022.106158.

Sou, T., Kaminskas, L.M., Nguyen, T.H., Carlberg, R., McIntosh, M.P., Morton, D.A.V., 2013. The effect of amino acid excipients on morphology and solid-state properties of multi-component spray-dried formulations for pulmonary delivery of biomacromolecules. Eur. J. Pharm. Biopharm. 83, 234–243. https://doi.org/10.1016/j.ejpb.2012.10.015.

Sun, D., 2020. Remdesivir for treatment of COVID-19: combination of pulmonary and IV administration may offer aditional benefit. AAPS J. 22 https://doi.org/10.1208/s12248-020-00459-8.

Tay, J.Y.S., Liew, C.V., Heng, P.W.S., 2018. Dissolution of fine particle fraction from truncated Anderson cascade impactor with an enhancer cell. Int. J. Pharm. 545, 45–50. https://doi.org/10.1016/j.ijpharm.2018.04.048.

Thorley, A.J., Tetley, T.D., 2013. New perspectives in nanomedicine. Pharmacol. Ther. https://doi.org/10.1016/j.pharmthera.2013.06.008.

Tse, J.Y., Kadota, K., Imakubo, T., Uchiyama, H., Tozuka, Y., 2021a. Enhancement of the extra-fine particle fraction of levofloxacin embedded in excipient matrix formulations for dry powder inhaler using response surface methodology. Eur. J. Pharm. Sci. 156, 105600 https://doi.org/10.1016/j.ejps.2020.105600.

Tse, J.Y., Koike, A., Kadota, K., Uchiyama, H., Fujimori, K., Tozuka, Y., 2021b. Porous particles and novel carrier particles with enhanced penetration for efficient pulmonary delivery of antitubercular drugs. Eur. J. Pharm. Biopharm. 167, 116–126. https://doi.org/10.1016/j.ejpb.2021.07.017.

Usmani, O.S., Biddiscombe, M.F., Barnes, P.J., 2005. Regional lung deposition and bronchodilator response as a function of β2-agonist particle size. Am. J. Respir. Crit. Care Med. 172, 1497–1504. https://doi.org/10.1164/rccm.200410-1414OC.

van Eerdenbrugh, B., Vermant, J., Martens, J.A., Froyen, L., van Humbeeck, J., Augustijns, P., Van Den Mooter, G., 2008. A screening study of surface stabilization during the production of drug nanocrystals. J. Pharm. Sci. 98, 2091–2103. https://doi.org/10.1002/jps.

Varga, P., Ambrus, R., Szabó-Révész, P., Kókai, D., Burián, K., Bella, Z., Fenyvesi, F., Bartos, C., 2021. Physico-chemical, *in vitro* and *ex vivo* characterization of meloxicam potassium-cyclodextrin nanospheres. Pharmaceutics 13, 1–14. https://doi.org/10.3390/pharmaceutics13111883.

Vargaftik, N.B., Volkov, B.N., Voljak, L.D., 1983. International tables of the surface tension of water. J. Phys. Chem. Ref. Data. https://doi.org/10.1063/1.555688.

Virók, D.P., Eszik, I., Mosolygó, T., Önder, K., Endrész, V., Burián, K., 2017. A direct quantitative PCR-based measurement of herpes simplex virus susceptibility to antiviral drugs and neutralizing antibodies. J. Virol. Methods 242, 46–52. https://doi.org/10.1016/j.jviromet.2017.01.007.

https://pubchem.ncbi.nlm.nih.gov/compound/Meloxicam. (Accessed 27 June 2022).

https://go.drugbank.com/drugs/DB00814. (Accessed 27 June 2022).